Tellus (2005), 57A, 55–64

TELLUS

An atmospheric balanced model of an axisymmetric vortex with zero potential vorticity

By THOMAS FRISIUS*, Institut für Meteorologie und Geophysik der Universität Frankfurt am Main, 60054 Frankfurt am Main, Germany

(Manuscript received 1 March 2004; in final form 28 June 2004)

ABSTRACT

This paper presents an atmospheric axisymmetric balanced model for a zero potential vorticity vortex that is vertically confined between two frictional boundary layers. Zero potential vorticity has the consequence that the potential temperature does not vary on angular momentum surfaces. This leads to neutrality with respect to symmetric instability. The axisymmetric balanced model conserves this flow property when the diabatic heating and the torque also do not vary on angular momentum surfaces. With these conditions and a transformation to the potential radius coordinates, the model reduces to prognostic equations for the physical radii at the lower and upper boundaries. The knowledge of these radii is sufficient to deduce all dynamic fields of the axisymmetric vortex. Analytical solutions can be obtained for vanishing viscosity and a prescribed heating profile. However, these solutions may reveal a frontal collapse in a finite time. This circumstance can be avoided by the inclusion of a horizontal diffusion term within the boundary layers. Then, the model produces a vortex resembling a tropical cyclone for a typical heating profile. It is suggested that the model might be used for a better conceptual understanding of tropical cyclogenesis.

1. Introduction

The potential vorticity (PV) theorem by Ertel (1942) proved to be very useful for the understanding of fluid dynamics in balanced models. An important implication is the invertibility principle, which states that all dynamic fields in a balanced model can be deduced from the PV distribution and the potential temperature at the boundaries (Hoskins et al. 1985). Therefore, we can derive dynamic fields solely by boundary values if the PV gradient vanishes everywhere. Perhaps the most significant analysis of such a uniform PV case stems from Eady (1949) with his model of baroclinic instability. Beside this work, there are many more illuminating studies on atmospheric uniform PV flows (e.g. Drazin 1970; Hoskins and Bretherton 1972; Hoskins 1976; Hoskins and West 1979; Blumen 1978; Shutts 1981; Emanuel 1986; Davies et al. 1991; Held et al. 1995).

The present paper deals with the special case of an axisymmetric vortex with zero PV. Such a vortex was first studied by Shutts (1981) to describe idealized hurricane structures. Zero PV implies that the absolute vorticity vector directs tangentially to isentropic surfaces. This condition is hardly fulfilled in the real atmosphere. However, implications may be drawn for convective vortices in which this condition is suitable for a PV based on saturated moist entropy (saturated moist PV). Indeed, the steady-state hurricane model of Emanuel (1986) assumes a zero saturated moist PV distribution. Furthermore, Hoskins and Bretherton (1972) stated that saturated moist PV almost vanishes in well-developed fronts. Shutts (1981) found that the essential structure of a hurricane vortex can even be described quite well for dry zero PV.

The condition of zero PV leads to neutrality with respect to symmetric instability (e.g. Eliassen and Kleinschmidt 1957). This condition is in accord with the so-called wind-induced surface heat exchange (WISHE) instability theory by Emanuel (1987), where the atmosphere is assumed to be always held in a hydrodynamically neutral state so that the convective heating is entirely controlled by surface heat fluxes. Therefore, a zero PV vortex model might be suitable for a rudimentary investigation of cyclogenesis by the WISHE mechanism. This issue will be investigated in a future study. The present paper introduces a balanced model of an axisymmetric zero PV vortex in a more general context and presents some simple applications where the convective heating is prescribed as an external forcing. The paper is structured as follows. Section 2 outlines the basic equations of the model, which are based on the transformed Eliassen balanced vortex model derived by Schubert and Hack (1983, hereafter SH83). In Section 3 these equations are drastically simplified by the assumption of vanishing PV. Then, the model consists of prognostic equations for the physical radii at the lower and upper boundaries. One can deduce all dynamical fields from the knowledge of the physical radii at these

*Corresponding author.
e-mail: frisius@meteor.uni-frankfurt.de

boundaries. Section 4 describes some simple solutions of the vortex model for a prescribed heat source. In Section 5 moist effects are considered by using the saturated moist entropy as the thermodynamic variable. Section 6 summarizes the outcome of this study.

2. Basic equations

The Eliassen balanced model (Eliassen 1951) describes a circular symmetric inviscid flow in a uniformly rotating atmosphere and assumes hydrostatic as well as gradient wind balance. In the present study, the inviscid atmosphere is coupled to horizontal boundary layers which lie below and above. The basic model equations are equivalent to those derived by SH83 with the exceptions that an upper boundary layer is introduced and that a torque is not excluded. The derivation in this section closely follows SH83.

2.1. Free atmosphere

The model uses the pressure-based pseudo-height coordinate introduced by Hoskins and Bretherton (1972). This vertical coordinate is given by

$$z = \left[1 - \left(\frac{p}{p_0}\right)^{(\gamma-1)/\gamma}\right] H_\mathrm{a}, \tag{1}$$

where p is the pressure, p_0 is a mean surface pressure and γ is the adiabatic exponent. H_a denotes the height where the pressure vanishes for an isentropic atmosphere having the reference potential temperature θ_0. As a result of the assumed circular symmetry, it is convenient to use cylindrical coordinates. Therefore, all fields can be expressed as functions of time t, radius r and pseudo-height z. The model equations for the free atmosphere are given by the gradient wind balance, angular momentum, hydrostatic balance, continuity and thermodynamic equations:

$$\frac{v^2}{r} + f v = \frac{\partial \phi}{\partial r}, \tag{2}$$

$$\frac{\partial M}{\partial t} + u\frac{\partial M}{\partial r} + w\frac{\partial M}{\partial z} = S_v r, \tag{3}$$

$$\frac{\partial \phi}{\partial z} = \frac{g}{\theta_0}\theta, \tag{4}$$

$$\frac{1}{r}\frac{\partial}{\partial r}(ru) + \frac{1}{\rho}\frac{\partial}{\partial z}(\rho w) = 0, \tag{5}$$

$$\frac{\partial \theta}{\partial t} + u\frac{\partial \theta}{\partial r} + w\frac{\partial \theta}{\partial z} = Q. \tag{6}$$

Here, u is the radial velocity, v is the tangential velocity, w is the vertical velocity, $M = vr + 1/2\, fr^2$ is the angular momentum per unit mass, θ is the potential temperature, ϕ is the geopotential, S_v is the momentum source for v, Q is the potential temperature tendency due to diabatic effects, f is the Coriolis parameter, and g is the acceleration due to gravity. The so-called pseudo-density ρ depends only on z and is given by

$$\rho(z) = \rho_0 \left(1 - \frac{z}{H_\mathrm{a}}\right)^{1/(\gamma-1)}. \tag{7}$$

The free atmosphere lies between two horizontal boundary layers at $z = 0$ and $z = H$. The coupling is established by the kinematic boundary conditions

$$w|_{z=0} = w_\mathrm{b}, \quad w|_{z=H} = w_\mathrm{t}, \quad v|_{z=0} = v_\mathrm{b}, \quad v|_{z=H} = v_\mathrm{t}, \tag{8}$$

where w_b (w_t) is the vertical velocity and v_b (v_t) is the tangential velocity at the top (bottom) of the lower (upper) boundary layer.

From the governing eqs. (2)–(6) one can derive the PV equation which is given by

$$\frac{\mathrm{d}q}{\mathrm{d}t} = \frac{\boldsymbol{\zeta}\cdot\nabla Q}{\rho} + \frac{\mathbf{e}_\lambda \cdot \nabla\theta \times \nabla(rS_v)}{r\rho} \quad \text{with} \quad q = \frac{1}{\rho}\,\boldsymbol{\zeta}\cdot\nabla\theta, \tag{9}$$

where $\mathbf{e}_\lambda$ denotes the unit vector in the tangential direction, q is the PV and $\boldsymbol{\zeta}$ is the absolute vorticity, which is related to the angular momentum by

$$\boldsymbol{\zeta} = -\frac{1}{r}\mathbf{e}_\lambda \times \nabla M. \tag{10}$$

The latter equation states that the vorticity vector is directed parallel to the angular momentum isolines, which is a well-known property of axisymmetric flows (e.g. Kleinschmidt 1951). The PV equation for $S_v = 0$ has the same form as the Ertel theorem Ertel (1942) applied for an axisymmetric vortex with the exception that in the Ertel law ρ and z are the real density and height, respectively. The PV equation states that PV will be conserved if the heat source Q and the torque rS_v do not vary along isolines of angular momentum and potential temperature, respectively. The present study is restricted to the special case where the PV vanishes always and everywhere. Therefore, isolines of angular momentum coincide with isentropes.

2.2. Boundary layers

Following SH83, local time derivatives are neglected in the thin boundary layers of vertical depth h. Furthermore, vertical independence of all variables except for the vertical velocity is assumed. Then, the tangential wind equation reduces to

$$\zeta_\mathrm{b} u_\mathrm{b} = D_\mathrm{b}, \qquad \zeta_\mathrm{t} u_\mathrm{t} = D_\mathrm{t}, \tag{11}$$

where ζ is the vertical component of absolute vorticity and D is the tangential frictional force. The subscripts 'b' and 't' denote that the variables are evaluated at $z = 0$ and $z = H$, respectively.

By integrating the continuity equation vertically, one can derive the vertical velocity at the top (bottom) of the lower (upper) boundary

$$w_{\mathrm{b}} = -\frac{h}{r}\frac{\partial}{\partial r}\left(r\frac{D_{\mathrm{b}}}{\zeta_{\mathrm{b}}}\right), \qquad w_{\mathrm{t}} = \frac{h}{r}\frac{\partial}{\partial r}\left(r\frac{D_{\mathrm{t}}}{\zeta_{\mathrm{t}}}\right), \tag{12}$$

where the vertical variation of pseudo-density has been neglected. These boundary conditions are needed for the coupling to the free atmosphere.

2.3. Transformation of the radius coordinate

For the present analysis it is necessary to transform the radius coordinate as in SH83. In this paper, the radius coordinate r is replaced by the so-called potential radius

$$R = \left(\frac{2}{f}vr + r^2\right)^{1/2} = \left(\frac{2}{f}M\right)^{1/2}. \tag{13}$$

The other coordinates remain unchanged but the letters T and Z are used instead of t and z to stress that R is held fixed when partial derivatives are applied.

The transformation leads after some algebra to the following closed set of equations (see SH83 for more details):

$$\frac{\partial r}{\partial T} + \frac{1}{f}\frac{r}{R}S_v\frac{\partial r}{\partial R} + \frac{1}{\rho}\frac{R}{r}\frac{\partial \psi^*}{\partial Z} = 0, \tag{14}$$

$$\frac{\partial \theta}{\partial T} + \frac{1}{f}\frac{r}{R}S_v\frac{\partial \theta}{\partial R} + \frac{q}{f}\frac{1}{R}\frac{\partial R\psi^*}{\partial R} = Q, \tag{15}$$

$$-f^2\frac{R^3}{r^3}\frac{\partial r}{\partial Z} = \frac{g}{\theta_0}\frac{\partial \theta}{\partial R}, \tag{16}$$

$$q = \frac{f}{\rho}\left(\frac{r}{R}\frac{\partial r}{\partial R}\right)^{-1}\frac{\partial \theta}{\partial Z}. \tag{17}$$

Here, ψ^* denotes the mass streamfunction of a modified transverse circulation given by $(\rho u^*, \rho w^*) = (r\rho/R(u - w\,\partial r/\partial Z), \rho f/\zeta\ w)$ which is non-divergent in transformed space. This holds even for $\dot{R} \neq 0$. Boundary values of ψ^* are needed to solve the system. The streamfunction vanishes at $R = 0$ and $R \to \infty$. The boundary conditions (12) can also be written in terms of ψ^*:

$$\psi^*_{\mathrm{b}} = -\rho_{\mathrm{b}}\frac{hr_{\mathrm{b}}^2}{fR^2}\frac{\partial r_{\mathrm{b}}}{\partial R}D_{\mathrm{b}}, \qquad \psi^*_{\mathrm{t}} = \rho_{\mathrm{t}}\frac{hr_{\mathrm{t}}^2}{fR^2}\frac{\partial r_{\mathrm{t}}}{\partial R}D_{\mathrm{t}}. \tag{18}$$

The ratio r/R appears several times in the transformed equation set. For large radii this ratio can be approximated by 1. By using this approximation and replacing $1/R\partial(R\psi^*)/\partial R$ with $\partial\psi^*/\partial R$ the model becomes equivalent to a semigeostrophic slab-symmetric model. A comparison with the slab-symmetric model may be useful to isolate the effects of curvature.

There are many more useful relations that can be derived in the transformed system (see SH83 and Thorpe 1985) but these are not needed in the present context. The conventional procedure to solve the system is to eliminate time tendencies from eqs. (14) and (15) to obtain a diagnostic equation for ψ^*. Solving this equation gives the velocity (u^*, w^*) that can be used to calculate time tendencies. The present study restricts the model to the special case of vanishing PV. Then, the equation set can be simplified further as will become clear in the following section.

3. Zero potential vorticity vortex model

By assuming vanishing PV and non-zero absolute vorticity one finds that

$$\frac{\partial \theta}{\partial Z} = 0. \tag{19}$$

Therefore, θ is vertically independent in transformed space and the integration of the thermal wind equation gives

$$r^2 = \left[\frac{1}{r_0^2} + \frac{2g}{f^2R^3\theta_0}\frac{\partial \theta}{\partial R}(Z - Z_0)\right]^{-1}, \tag{20}$$

where r_0 denotes the physical radius at the height Z_0. Therefore, angular momentum isolines have $1/r^2$ shape in the physical (r, z)-space where the contours slope outward (inward) for a warm (cold) core vortex.

On the other hand, vertical integration of eq. (14) multiplied with $\rho\, r$ gives

$$\left(\frac{\partial}{\partial T} + \dot{R}\frac{\partial}{\partial R}\right)F = R(\psi^*_{\mathrm{b}} - \psi^*_{\mathrm{t}}), \tag{21}$$

where

$$F = \int_0^H \frac{r^2}{2}\rho\,\mathrm{d}Z \text{ and } \dot{R} = \frac{r_{\mathrm{b}}S_v}{Rf}.$$

For the derivation of eq. (21) it was assumed that the radial velocity in transformed space R does not vary along angular momentum isolines in order to ensure PV conservation. The integral quantity F is proportional to the mass inside the respective angular momentum surface. The mass can be changed by mass fluxes at the upper and lower boundaries or by a change of angular momentum due to the torque rS_v. Because of the integrated thermal wind eq. (20), one can also express F as a function of $r_0 = r|_{Z=Z_0}$ and $G(R, T) = 2\,g/(f^2R^3\theta_0)\partial\theta/\partial R$:

$$F(r_0, G) = \frac{1}{2}\int_0^H \frac{\rho}{r_0^{-2} + G(Z - Z_0)}\mathrm{d}Z. \tag{22}$$

This leads to the following prognostic equation for the physical radius r_0

$$\frac{\partial r_0}{\partial T} + \dot{R}\frac{\partial r_0}{\partial R} = \frac{2g}{f^2\theta_0R^3}\left[\frac{1}{R^3}\frac{\partial(R^3\dot{R})}{\partial R}\frac{\partial \theta}{\partial R} - \frac{\partial Q}{\partial R}\right]\frac{\partial F}{\partial G}\bigg/\frac{\partial F}{\partial r_0} + R(\psi^*_{\mathrm{b}} - \psi^*_{\mathrm{t}})\bigg/\frac{\partial F}{\partial r_0}, \tag{23}$$

which can be integrated by knowing the upper and lower boundary values of ψ^*. Therefore, it is suitable to evaluate this equation at the upper and lower boundaries. By doing this and noting that

$$G = \frac{2g}{f^2R^3\theta_0}\frac{\partial\theta}{\partial R} = \frac{1}{H}\left(\frac{1}{r_t^2} - \frac{1}{r_b^2}\right) = \frac{1}{H}\frac{r_b^2 - r_t^2}{r_b^2 r_t^2} \tag{24}$$

one arrives at the following two equations:

$$\frac{\partial r_b}{\partial T} + \dot{R}\frac{\partial r_b}{\partial R} = \left[\frac{1}{R^3}\frac{\partial(R^3\dot{R})}{\partial R}\frac{r_b^2 - r_t^2}{Hr_b^2r_t^2} - \frac{2g}{f^2R^3\theta_0}\frac{\partial Q}{\partial R}\right] \times \left.\frac{\partial F}{\partial G}\right|_{r_b} \Big/ \left.\frac{\partial F}{\partial r_b}\right|_G + R(\psi_b^* - \psi_t^*) \Big/ \left.\frac{\partial F}{\partial r_b}\right|_G, \tag{25}$$

$$\frac{\partial r_t}{\partial T} + \dot{R}\frac{\partial r_t}{\partial R} = \left[\frac{1}{R^3}\frac{\partial(R^3\dot{R})}{\partial R}\frac{r_b^2 - r_t^2}{Hr_b^2r_t^2} - \frac{2g}{f^2R^3\theta_0}\frac{\partial Q}{\partial R}\right] \times \left.\frac{\partial F}{\partial G}\right|_{r_t} \Big/ \left.\frac{\partial F}{\partial r_t}\right|_G + R(\psi_b^* - \psi_t^*) \Big/ \left.\frac{\partial F}{\partial r_t}\right|_G \tag{26}$$

These two equations form the zero PV vortex model and can be integrated when S_v, Q, D_b and D_t are suitably parametrized. For a realistic value of γ (γ is nearly 7/5 in the atmosphere) the integral (22) leads to a rather complicated function. The necessary integrals for $\gamma = 7/5$ are given in the appendix. The present paper concentrates on the Boussinesq approximation where ρ is assumed to be constant and coincides with the density ρ_0 at $Z = 0$. This simplification makes the model more transparent and is satisfactory for conceptual purposes. Then, the model equations take the form:

$$\begin{aligned}\frac{\partial r_b}{\partial T} + \dot{R}\frac{\partial r_b}{\partial R} = {}&\left[\frac{1}{R^3}\frac{\partial(R^3\dot{R})}{\partial R}\frac{r_b^2 - r_t^2}{Hr_b^2r_t^2} - \frac{2g}{f^2\theta_0R^3}\frac{\partial Q}{\partial R}\right] \\ &\times\frac{r_b^3r_t^2H}{2r_b^2 - 2r_t^2}\left[1 - \frac{r_b^2}{r_b^2 - r_t^2}\ln\left(\frac{r_b^2}{r_t^2}\right)\right] \\ &-\frac{h}{H}\frac{r_b}{fr_t^2R}\left(r_b^2\frac{\partial r_b}{\partial R}D_b + r_t^2\frac{\partial r_t}{\partial R}D_t\right),\end{aligned} \tag{27}$$

$$\begin{aligned}\frac{\partial r_t}{\partial T} + \dot{R}\frac{\partial r_t}{\partial R} = {}&\left[\frac{1}{R^3}\frac{\partial(R^3\dot{R})}{\partial R}\frac{r_t^2 - r_b^2}{Hr_b^2r_t^2} + \frac{2g}{f^2\theta_0R^3}\frac{\partial Q}{\partial R}\right] \\ &\times\frac{r_t^3r_b^2H}{2r_t^2 - 2r_b^2}\left[1 - \frac{r_t^2}{r_t^2 - r_b^2}\ln\left(\frac{r_t^2}{r_b^2}\right)\right] \\ &-\frac{h}{H}\frac{r_t}{fr_b^2R}\left(r_b^2\frac{\partial r_b}{\partial R}D_b + r_t^2\frac{\partial r_t}{\partial R}D_t\right).\end{aligned} \tag{28}$$

The treatment of the first terms on the right-hand sides of both equations becomes numerically difficult when $r_b \to r_t$, i.e. the temperature gradient almost vanishes. Then, it is suitable to expand them in a Taylor series leading to the approximations

$$\frac{r_b^3r_t^2H}{2r_b^2 - 2r_t^2}\left[1 - \frac{r_b^2}{r_b^2 - r_t^2}\ln\left(\frac{r_b^2}{r_t^2}\right)\right] \approx -\frac{r_b^3H}{2}\left[\frac{1}{2} - \frac{1}{6}\left(\frac{r_b^2}{r_t^2} - 1\right)\right] \tag{29}$$

and

$$\frac{r_t^3r_b^2H}{2r_t^2 - 2r_b^2}\left[1 - \frac{r_t^2}{r_t^2 - r_b^2}\ln\left(\frac{r_t^2}{r_b^2}\right)\right] \approx -\frac{r_t^3H}{2}\left[\frac{1}{2} - \frac{1}{6}\left(\frac{r_t^2}{r_b^2} - 1\right)\right]. \tag{30}$$

These approximations are valid as long as $\mid r_b^2 - r_t^2 \mid \ll (r_b^2 + r_t^2)/2$, and find application when the temperature gradient becomes small or the physical radii are very large. In the case of uniform PV, one can deduce all dynamic fields from boundary values. In the present model the knowledge of the physical radii is sufficient. The following relations can be used to calculate all important dynamic fields:

$$r^2 = \left[\frac{1}{r_b^2} + \frac{Z}{H}\left(\frac{1}{r_t^2} - \frac{1}{r_b^2}\right)\right]^{-1}, \tag{31}$$

$$\frac{\partial\theta}{\partial R} = \frac{f^2R^3\theta_0}{2gH}\left(\frac{1}{r_t^2} - \frac{1}{r_b^2}\right), \tag{32}$$

$$v = \frac{f}{2}\frac{R^2 - r^2}{r}, \tag{33}$$

$$\zeta = f\frac{R}{r}\left(\frac{\partial r}{\partial R}\right)^{-1}, \tag{34}$$

$$\theta = -\int_R^\infty \frac{\partial\theta}{\partial R}\mathrm{d}R + \lim_{R\to\infty}\theta, \tag{35}$$

$$\begin{aligned}\frac{\psi^*}{\rho_0} = {}&\frac{\psi_b^*}{\rho_0} + \frac{1}{2GR}\left[\frac{\partial Q}{\partial R}\Big/\frac{\partial\theta}{\partial R} - \frac{1}{R^3}\frac{\partial(R^3\dot{R})}{\partial R}\right]\ln(1 + Gr_b^2Z) \\ &-\left\{\left[\frac{\partial Q}{\partial R}\Big/\frac{\partial\theta}{\partial R} - \frac{1}{R^3}\frac{\partial(R^3\dot{R})}{\partial R}\right]r_b^2Z \right.\\ &\left.+2\left(\frac{\partial r_b}{\partial T} + \dot{R}\frac{\partial r_b}{\partial R}\right)r_bZ\right\}\left[2R(1 + Gr_b^2Z)\right]^{-1},\end{aligned} \tag{36}$$

$$\rho_0 w = \frac{\zeta}{f}\frac{1}{R}\frac{\partial}{\partial R}\left(R\psi^*\right), \tag{37}$$

$$\rho_0 u = -\frac{R}{r}\frac{\partial\psi^*}{\partial Z} + w\frac{\partial r}{\partial Z}. \tag{38}$$

4. Some simple solutions

4.1. Inviscid case

Further simplifications emerge when the boundary layers and the torque are excluded. Then, the prognostic equations for the physical radii take the form:

$$\frac{\partial r_b}{\partial T} = -\frac{gH}{f^2\theta_0R^3}\frac{r_b^3r_t^2}{r_b^2 - r_t^2}\left[1 - \frac{r_b^2}{r_b^2 - r_t^2}\ln\left(\frac{r_b^2}{r_t^2}\right)\right]\frac{\partial Q}{\partial R}, \tag{39}$$

$$\frac{\partial r_t}{\partial T} = \frac{gH}{f^2\theta_0 R^3}\frac{r_t^3 r_b^2}{r_t^2 - r_b^2}\left[1 - \frac{r_t^2}{r_t^2 - r_b^2}\ln\left(\frac{r_t^2}{r_b^2}\right)\right]\frac{\partial Q}{\partial R}. \tag{40}$$

These equations do not include spatial derivatives except for the term $\partial Q/\partial R$. For a prescribed $\partial Q/\partial R$, analytical solutions can be found. However, this apparent advantage of the inviscid model is accompanied by the possibility of a frontal collapse in a finite time. This occurs when

$$\frac{\partial r}{\partial R} = 0, \tag{41}$$

i.e. absolute vorticity becomes infinite. The possibility of a frontal collapse is a well-known property of two-dimensional models based on the geostrophic momentum equations. This was found by Hoskins and Bretherton (1972) by investigating frontogenesis in a horizontal deformation flow. The effect of this 'external' flow can be interpreted as a momentum forcing $\dot{R} \neq 0$ acting on the frontal-scale flow (see their eq. 3.6). They showed amongst other things that a frontal collapse results for a zero PV frontal-scale flow. Therefore, momentum forcing $\dot{R} \neq 0$ together with $Q = 0$ may lead to a frontal collapse as well as differential heating $\partial Q/\partial R \neq 0$ with $\dot{R} = 0$. The latter will be demonstrated in the following.

The analytical solution of the inviscid model can be obtained by recalling that the mass term F will be conserved in the inviscid case. F can be expressed as

$$F(r_b, G) = \frac{\rho_0}{2G}\ln(1 + Gr_b^2 H) \tag{42}$$

or

$$F(r_t, G) = -\frac{\rho_0}{2G}\ln(1 - Gr_t^2 H). \tag{43}$$

Therefore, one obtains

$$r_b = \left\{\frac{f^2R^3\theta_0}{2gH}\left[\exp\left(\frac{4gF}{\rho_0 f^2R^3\theta_0}\frac{\partial\theta}{\partial R}\right) - 1\right]\Big/\frac{\partial\theta}{\partial R}\right\}^{1/2}, \tag{44}$$

$$r_t = \left\{\frac{f^2R^3\theta_0}{2gH}\left[1 - \exp\left(-\frac{4gF}{\rho_0 f^2R^3\theta_0}\frac{\partial\theta}{\partial R}\right)\right]\Big/\frac{\partial\theta}{\partial R}\right\}^{1/2}, \tag{45}$$

where $\theta = \theta|_{T=0} + \int_0^T Q\,\mathrm{d}T$ and $F = \rho_0 \int_0^H 1/2r^2 \,|_{T=0}\,\mathrm{d}Z$.

The occurrence of a frontal collapse can be estimated by the radial derivatives of the squared physical radius. These are given by

$$\frac{\partial r_b^2}{\partial R} = \frac{1}{G^2H}\left[\left(\frac{2FG}{\rho_0} - 1\right)\mathrm{e}^{2FG/\rho_0} + 1\right]\frac{\partial G}{\partial R} + \frac{2}{\rho_0 H}\mathrm{e}^{2FG/\rho_0}\frac{\partial F}{\partial R}, \tag{46}$$

$$\frac{\partial r_t^2}{\partial R} = \frac{1}{G^2H}\left[\left(\frac{2FG}{\rho_0} + 1\right)\mathrm{e}^{-2FG/\rho_0} - 1\right]\frac{\partial G}{\partial R} + \frac{2}{\rho_0 H}\mathrm{e}^{-2FG/\rho_0}\frac{\partial F}{\partial R}. \tag{47}$$

The second terms on the right-hand sides of these equations always take a positive value because the mass term F monotonically grows with increasing potential radius. The factor before $\partial G/\partial R$ has a positive value in eq. (46) and a negative value in eq. (47). Therefore, a frontal collapse cannot take place both at the lower and upper boundaries for the same potential radius. The radial derivative of G takes the form

$$\frac{\partial G}{\partial R} = \frac{2g}{f^2R^3\theta_0}\left(\frac{\partial^2\theta}{\partial R^2} - \frac{3}{R}\frac{\partial\theta}{\partial R}\right). \tag{48}$$

Consequently, for a warm core vortex with $\partial\theta/\partial R < 0$ a frontal collapse will be more likely at the upper boundary because $\partial^2\theta/\partial R^2$ and $-\partial\theta/\partial R$ are both positive in the outer part of the vortex, but negative values of $\partial G/\partial R$ are less likely because of the negative temperature gradient. For example, the heating profile $Q = Q_0\exp(-R^2/R_0^2)$ cannot cause a frontal collapse at the lower boundary. If, on the other hand, heating appears at some distance from the vortex center (as, for example, in the eyewall of a tropical cyclone) a lower boundary frontal collapse will be very probable. This has already been pointed out by Emanuel (1997) who found that the inner edge of the tropical cyclone's eyewall is strongly frontogenetic.

In the following some simple solutions of the model are presented where the model constants are chosen to be

$$f = 0.5 \times 10^{-4}\frac{1}{\mathrm{s}}, \quad \theta_0 = 273\ \mathrm{K} \quad \text{and} \quad H = 10000\ \mathrm{m}.$$

Figure 1 displays the evolution of the upper and lower boundary vorticity maxima for

$$Q = Q_0\exp\left(-\frac{R^2}{R_0^2}\right), \tag{49}$$

where $R_0 = 250$ km and $Q_0 = 1\ \mathrm{K\ d^{-1}}$. The solid and dashed lines show the evolution when the initial flow is at rest, whereas

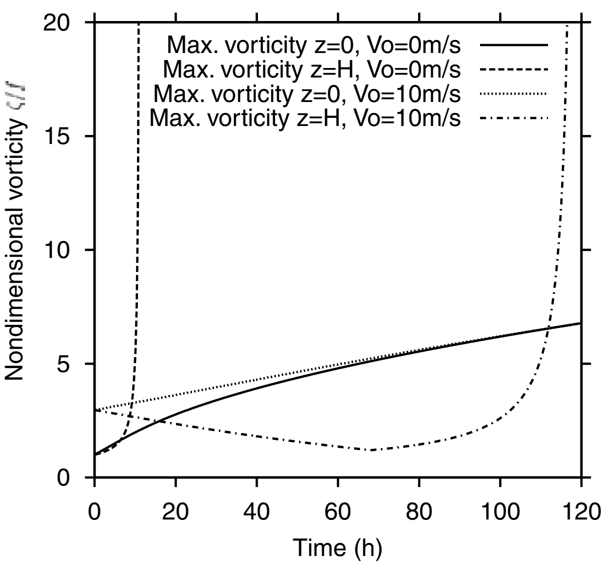

Fig 1. Time evolution of vorticity maxima for the solutions with maximum heating at $R = 0$. The solid and dashed lines show the lower and upper boundary vorticity maxima, respectively, for the solution without an initial vortex. The dotted and dot-dashed lines display the corresponding results for the solution with an initial barotropic vortex.

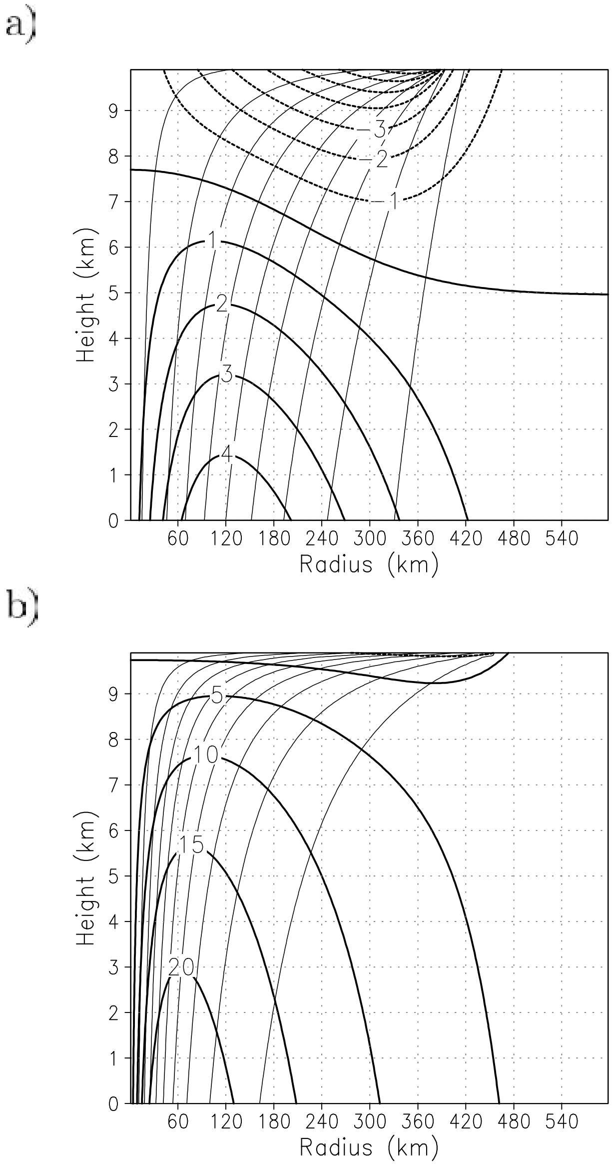

Fig 2. Radius–height cross-section in physical space for tangential wind (thick lines) and potential temperature (thin lines). (a) Solution without initial vortex at $t = 10$ h (contour interval 1 m s^{-1} for tangential wind and 0.05 K for potential temperature). (b) Solution with an initial barotropic vortex at $t = 118$ h (contour interval 5 m s^{-1} for tangential wind and 0.5 K for potential temperature).

the dotted and dashed lines represent the results for an initial barotropic vortex with $v = v_0 R/R_0 \exp[-(R^2/R_0^2 - 1)/2]$ where $v_0 = 10$ m s^{-1}. A frontal collapse occurs at the upper boundary at $t = 11$ h for the solution without an initial vortex and at $t = 118$ h for the solution including the initial vortex. Therefore, the presence of an initial vortex delays the frontal collapse considerably due to the stronger inertial vortex stability. Figure 2 shows the tangential wind and potential temperature at a time just before the frontal collapse takes place. The solution without an initial vortex (Fig. 2a) only achieved a maximum wind of 5 m s^{-1} at the surface at a physical radius of about 110 km. The maximum upper level anticyclonic flow lies at a much larger physical radius and has a somewhat larger magnitude than the lower level cyclonic flow. The frontal collapse at the upper boundary arises due the strong radial displacements of the isentropes. For the solution with an initial vortex (Fig. 2b) the cyclonic winds are much stronger than the anticyclonic winds. Now, the wind structure much more resembles that of a tropical cyclone vortex although the intensity is too weak. Similar heating profiles were used by Hack and Schubert (1986) and Schubert and Alworth (1987) in the Eliassen balanced model but with a stronger forcing. Nevertheless, they obtain a similar vortex amplification because their model starts with a stably stratified atmosphere. Then, a larger fraction of heating will be used up to generate potential energy that cannot be converted to kinetic energy. They detect no frontal collapse, presumably because they have a flexible tropopause instead of a rigid lid.

To see the effect of a heating maximum at a finite radius, another solution is described here for which the heating is given by

$$Q = Q_0 \frac{R^2}{R_0^2} \exp\left(-\frac{R^2}{R_0^2} + 1\right), \tag{50}$$

where R_0 and Q_0 take the same values as before. Then, the maximum heating is located at $R = 250$ km. Figure 3a displays the evolution of the corresponding vorticity maxima. It can be seen that the heating profile produces a frontal collapse first at the lower boundary and afterwards at the upper boundary. In Fig. 3b, showing tangential wind and temperature just before the front collapses, it can be seen that the lower boundary front formed just inside of the radius of the heating maximum. Because of the positive radial temperature gradient, the flow is anticyclonic at the lower boundary near the vortex centre. Such a pattern is rather unlikely for real tropical cyclones because adiabatic warming by subsidence in the eye of a tropical cyclone prevents the development of a negative temperature gradient. In the zero PV vortex model, adiabatic warming cannot take place due to the neutral stratification at the vortex axis.

4.2. *Effect of the density profile*

This subsection examines the effect of a vertically decreasing pseudo density given by eq. (7) for $\gamma = 7/5$. The expression for F is given in the appendix. Because it is not possible to determine r_b and r_t analytically, a Newton iteration method is used. The absolute height H_a of the atmosphere is chosen to be 28 000 m. It appears that the upper (lower) boundary frontal collapse takes place earlier (later) than in the corresponding Boussinesq approximated solutions. Such a behaviour results because the mass conservation requires a stronger outflow and a weaker inflow for the same vertical velocity profile when density decreases with height. This is confirmed by Fig. 4, which displays the tangential

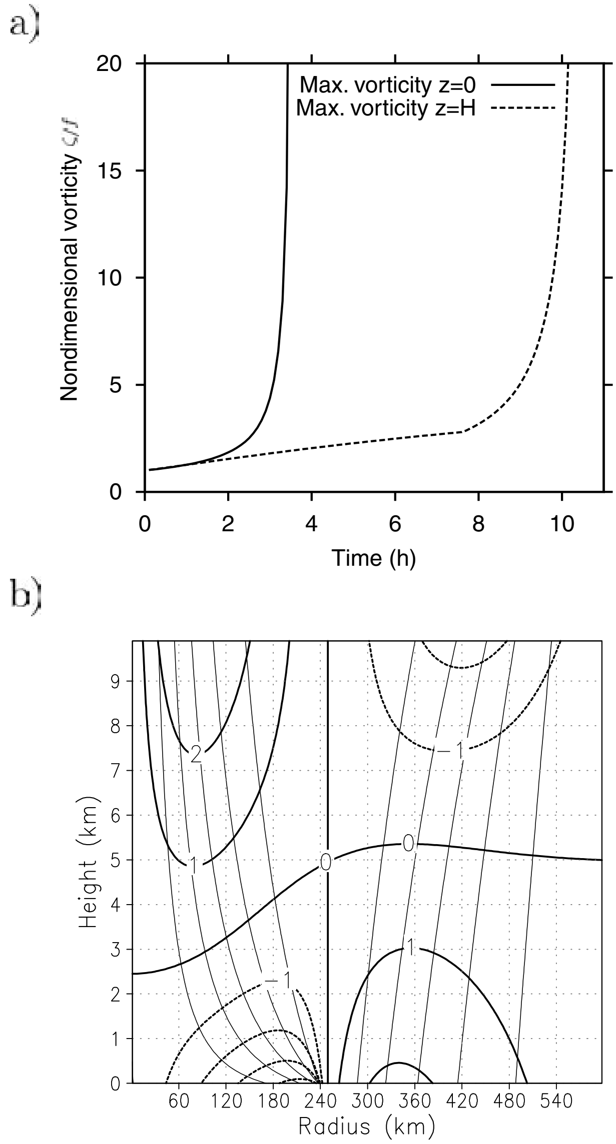

Fig 3. Results for the solution with maximum heating at $R = 250$ km. (a) The solid and dashed lines show the lower and upper boundary vorticity maxima, respectively. (b) Radius–height cross-section in physical space for tangential wind (thick lines) and potential temperature (thin lines) at $t = 3$ h (contour interval 1 m s^{-1} for tangential wind and 0.025 K for potential temperature).

wind extrema as a function of time for the heating profile (49). Figure 4 also shows the results for the corresponding Boussinesq solution. It becomes evident that the maximum tangential wind is always weaker (stronger) at the lower (upper) boundary than in the corresponding Boussinesq solution.

4.3. Effect of horizontal diffusion

It is useful to include a horizontal diffusion term to prevent a frontal collapse. On the other hand, diffusion is not consistent with the zero PV assumption when it acts outside the boundary layers. Therefore, to avoid the generation of PV, diffusion should be restricted to the boundary layer and contained in the drag terms D_b and D_t. Nevertheless, in the real atmosphere, turbulent diffusion might occur outside the boundary layer due to deep convection or shear instabilities. Nakamura and Held (1989) found that horizontal diffusion generates positive PV near a frontal zone. However, the localized generation of PV is possibly not so relevant for the broad vortex structure so that the zero PV assumption is quite acceptable for a simple conceptual model. A simple formulation for horizontal diffusion at the lower and upper boundaries is given by

$$D_j = \frac{1}{r_j^2}\frac{\partial}{\partial r_j}\left[k r_j^3 \frac{\partial}{\partial r_j}\left(\frac{v}{r_j}\right)\right]$$
$$= \frac{f}{2r_j^2}\frac{\partial}{\partial r_j}\left[k r_j^3 \frac{\partial}{\partial r_j}\left(\frac{R^2}{r_j^2}\right)\right] \quad \text{for } j = b, t, \tag{51}$$

where k denotes an eddy diffusion coefficient. Because the mass term F will not be conserved any more, the solution must be obtained by numerical integration of eqs. (27) and (28). A numerical solution will be presented in the following for a constant eddy diffusion coefficient of $k = 2 \times 10^4$ m^2 s^{-1} and a radial gridpoint distance of *3* km in transformed space. For lower values of k, the numerical solution produces a frontal collapse. However, this event seems to result from the numerical scheme rather than from the true solution of the model. First, the heating profile (49) is considered. Figure 5a displays the evolution of the upper and lower boundary vorticity maximum for the numerical

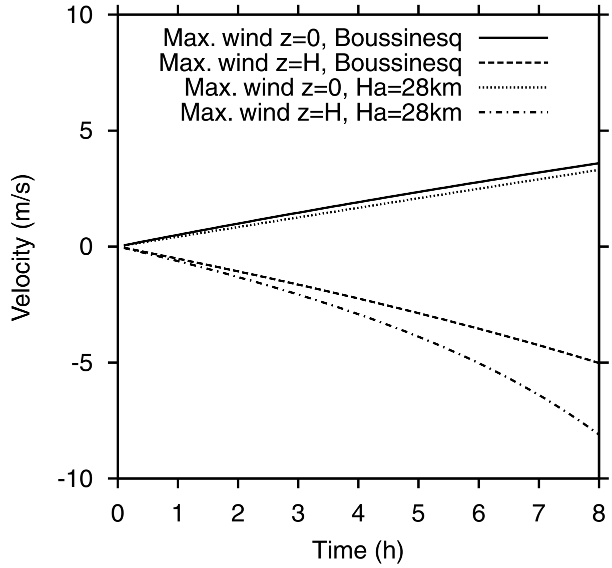

Fig 4. Time evolution of the tangential wind extrema for solutions with maximum heating at $R = 0$. The solid and dashed lines show the lower and upper boundary tangential wind extrema, respectively, for the Boussinesq-approximated model. The dotted and dot-dashed lines display the corresponding results for an atmosphere with $\gamma = 7/5$ and $H_a = 28\,000$ m.

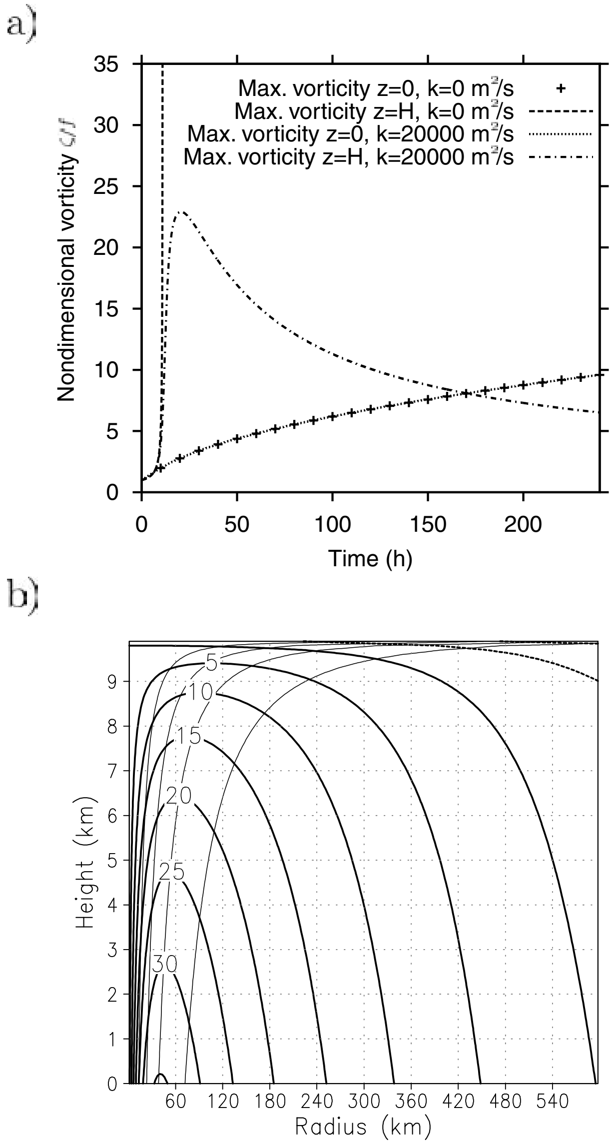

Fig 5. Results for the solution with horizontal diffusion and maximum heating at $R = 0$. (a) The crosses and the dashed line show the lower and upper boundary vorticity maxima without diffusion, respectively. The dotted and dot-dashed lines display the corresponding results for $k = 20\,000$ m^2 s^{-1}. (b) Radius–height cross-section in physical space for tangential wind (thick lines) and potential temperature (thin lines) at $t = 240$ h for $k = 20\,000$ m^2 s^{-1} (contour interval 5 m s^{-1} for tangential wind and 2 K for potential temperature).

solution with diffusion and the analytical solution without diffusion. With diffusion, the upper boundary vorticity maximum reaches a value of about $23f$ at $t = 20$ h and declines afterwards. Surprisingly, the development of the lower boundary vorticity maximum nearly coincides with that of the solution without diffusion. Also, the lower boundary tangential wind profiles (not shown) are very similar to the case without diffusion, except for some differences in the outer part of the vortex. Therefore, the

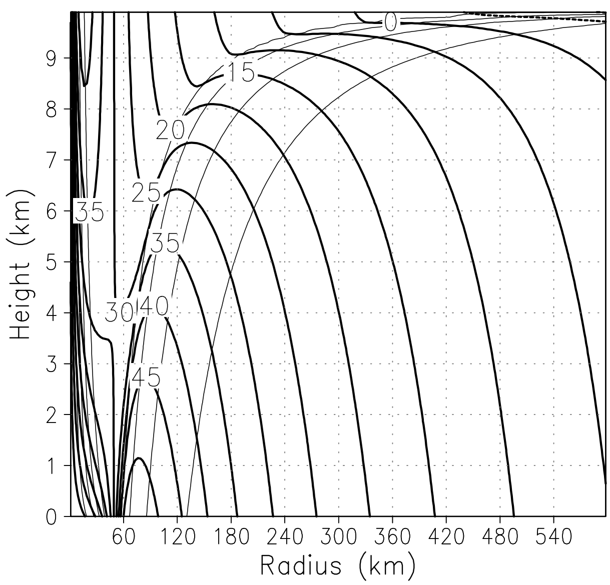

Fig 6. As in Fig. 5b but for the solution with maximum heating at $R = 250$ km and a diffusion coefficient of $k = 80\,000$ m^2 s^{-1} (contour interval 5 m s^{-1} for tangential wind and 2 K for potential temperature).

details of the upper boundary front do not have much influence on the evolution of the lower boundary wind profile. Figure 5b displays the tangential wind and potential temperature in physical space at $t = 240$ h. This vortex has a maximum tangential velocity of 35 m s^{-1}. The vortex structure is comparable to real tropical cyclones with strong surface winds at a small radius and a weak upper level anticyclonic flow in the outer part of the vortex. Figure 6 shows the corresponding tangential wind and potential temperature fields at $t = 240$ h for a simulation based on the heating profile (50). Now, the eddy diffusion coefficient amounts to $\nu = 8 \times 10^4$ m^2 s^{-1}. This high value was necessary to prevent a frontal collapse at the lower boundary. For radii larger than 60 km, the vortex also resembles the structure of a real tropical cyclone. However, the inner core consists of a small-scale cyclonic wind maximum at the upper boundary which does not appear in reality (see, for example, Anthes 1982). This discrepancy can be explained by the absence of adiabatic warming due to subsidence at the origin in the present model. Therefore, a temperature minimum always emerges instead of a maximum when heating takes place at a finite radius.

5. Consideration of moist effects

Moist effects can be incorporated in the present model when a saturated atmosphere is assumed and when saturated moist entropy does not vary along angular momentum surfaces. Emanuel (1986) found that the thermal wind balance equation in transformed space can be written as

$$f^2 \frac{R^3}{r^3} \frac{\partial r}{\partial P} = \frac{\partial \mathcal{T}}{\partial P} \frac{\partial s^*}{\partial R}, \tag{52}$$

where $\partial/\partial P$ is the derivative with respect to pressure along an angular momentum surface, $\mathcal{T}$ denotes the temperature and s^* is the saturated moist entropy. The latter quantity is approximately conserved in a saturated atmosphere. The transformation to pseudo-height is straightforward because it is also based on pressure. Therefore,

$$f^2 \frac{R^3}{r^3} \frac{\partial r}{\partial Z} = \frac{\partial \mathcal{T}}{\partial Z} \frac{\partial s^*}{\partial R}. \tag{53}$$

For conceptual purposes one can treat $\Gamma =: -\partial \mathcal{T}/\partial Z$ as a constant. In the saturated moist model eqs. (14) and (15) remain the same, with the difference that θ has to be replaced by s^* and Q is the source for moist entropy instead of diabatic heating. Q would approximately vanish when air ascends in a saturated environment. It can be imagined as the convective flux convergence of moist air from the lower boundary layer. The PV must be replaced by the saturated moist PV defined as

$$q = \frac{f}{\rho} \left(\frac{r}{R} \frac{\partial r}{\partial R} \right)^{-1} \frac{\partial s^*}{\partial Z}, \tag{54}$$

which becomes zero because moist entropy does not vary along angular momentum surfaces. The final model equations take the same form as eqs. (25) and (26) with the only differences that Γ and s^* replace g/θ_0 and θ, respectively.

Although the condition that saturated moist entropy does not vary along angular momentum surfaces is reasonable for the eyewall of a tropical cyclone, the moist model still has some limitations. Real tropical cyclones contain an eye where dry unsaturated air subsides. There, saturated moist entropy is not a conserved variable and a source for saturated moist PV comes into play. If the maximum convective flux occurs at a finite radius, the moist model will predict a temperature minimum at the vortex centre as in the dry model. Normally, adiabatic warming by subsidence in the eye prevents the temperature minimum. Furthermore, much downward motion in unsaturated air occurs also at other places than in the tropical cyclone's eye. However, Willoughby et al. (1984) found, in an axisymmetric tropical cyclone model, that the exclusion of ice-phase microphysics highly suppresses such downdrafts but still allows the evolution of a hurricane vortex. As a consequence, the atmosphere of the inner part of the hurricane vortex is saturated nearly everywhere except for the eye (see their fig. 6). Consequently, the assumption of a saturated atmosphere outside the eye and outside the boundary layer is reasonable for an idealized tropical cyclone model.

6. Conclusion

This paper introduces a balanced vortex model based on the assumption that PV vanishes everywhere. This assumption leads to a drastic simplification of the governing equations to two prognostic equations for the physical radii at the lower and upper boundaries. For vanishing mass fluxes at these boundaries and a prescribed heating profile, analytical solutions can be found. Some simple examples reveal a likely appearance of a frontal collapse for heating profiles that are typical for tropical cyclones. The timing of this collapse increases considerably when a barotropic cyclone is initially present. The inclusion of horizontal diffusion in the adjacent boundary layers prevents the frontal collapse and makes it possible that the model generates a vortex like a tropical cyclone. The assumption zero PV is somewhat unrealistic because in real tropical cyclones PV has normally a positive non-zero value due to the stable stratification. However, the model can also be interpreted in a different way when saturated moist entropy is used as the thermodynamic variable. Then, the atmosphere has a moist neutral stratification that corresponds much better with the conditions in real tropical cyclones. It is assumed that the atmosphere is saturated everywhere with vanishing saturated moist PV. This assumption was also made in Emanuel's steady-state model of a tropical cyclone (Emanuel 1986). With the zero PV vortex model, one has the possibility of investigating the development of an idealized tropical depression in a moist neutral environment. However, the model lacks the dry adiabatic warming in the tropical cyclone eye. This lack leads to the formation of a lower boundary anticyclone when the heating appears at a finite radius. Possibly, this circumstance might be prevented by introducing a pseudo-heating of the form $Q = -c/H \int_0^H w \, dZ$ to crudely represent the adiabatic warming in regions where the air is not saturated. Note that the dry limit of the moist model does not agree with the dry model when subsaturation would be allowed. This is explained by the fact that the dry limit of saturated moist PV does not lead to the classical dry PV (Schubert 2004). Therefore, the model approach is not useful for general applications where both moist and dry dynamics are important. On the other hand, a PV based on moist entropy or equivalent potential temperature has the correct dry limit but is not invertible (Schubert 2004) and cannot be used in the present model.

Emanuel (1989) – see also Emanuel (1995) – presented a simple tropical cyclone model which has some features in common with the present zero PV model. Emanuel's model includes a thought-out parametrization of convection and can properly simulate the development of a tropical cyclone in a moist neutral environment. The model is also based on prognostic equations for the physical radii at the lower and upper boundaries and assumes zero saturated moist PV. In contrast to the present model, the vertical derivative of the streamfunction is approximated with a finite difference to calculate the radial velocity. Furthermore, an elliptic equation to determine the streamfunction must still be solved which is not necessary here.

To study cyclogenesis by the WISHE mechanism in the zero PV model, one has to parametrize Q and $\dot{R}$ suitably. Surely, it is necessary to include an additional equation for the boundary layer temperature or saturation moist entropy as, for example, in the model of Emanuel (1995). This issue will be treated in a future study.

7. Acknowledgments

The author thanks two anonymous reviewers for their valuable comments.

8. Appendix

The mass term F can be integrated for a deep atmosphere when $\gamma = 7/5$. Then, F expressed as a function of r_b and G becomes

$$
\begin{aligned}
F(r_b, G) &= \int_0^H \frac{1}{2} \frac{\rho_0 [1-(Z/H_a)]^{5/2}}{1/r_b^2 + GZ} \mathrm{d}Z \\
&= \frac{H_a \rho_b r_b^2}{2} \left[\frac{30 + 70A_b + 46A_b^2}{15A_b^3} \left(\sqrt{1 - \frac{H}{H_a}} - 1 \right) \right. \\
&\quad - \left(\frac{10 + 22A_b}{15A_b^2} - \frac{2}{5A_b} \frac{H}{H_a} \right) \\
&\quad \times \frac{H}{H_a} \sqrt{1 - \frac{H}{H_a}} - \frac{2(1 + A_b)^{5/2}}{A_b^{7/2}} \left\{ \mathrm{artanh} \right. \\
&\quad \left. \left. \times \left[\frac{\sqrt{A_b}}{\sqrt{1 + A_b}} \frac{\sqrt{1 - (H/H_a)} - 1}{1 - A_b/(1 + A_b)\sqrt{1 - (H/H_a)}} \right] \right\} \right]
\end{aligned} \tag{A1}
$$

where $A_b = H_a G r_b^2$. A similar expression results for F expressed as a function of r_t and G:

$$
\begin{aligned}
F(r_t, G) &= \int_0^H \frac{1}{2} \frac{\rho_0 [1-(Z/H_a)]^{5/2}}{1/r_t^2 + G(Z - H)} \mathrm{d}Z \\
&= \frac{H'_a \rho_t r_t^2}{2} \left[\frac{30 + 70A_t + 46A_t^2}{15A_t^3} \left(1 - \sqrt{1 + \frac{H}{H'_a}} \right) \right. \\
&\quad - \left(\frac{10 + 22A_t}{15A_t^2} + \frac{2}{5A_t} \frac{H}{H'_a} \right) \\
&\quad \times \frac{H}{H'_a} \sqrt{1 + \frac{H}{H'_a}} + \frac{2(1 + A_t)^{5/2}}{A_t^{7/2}} \left\{ \mathrm{artanh} \right. \\
&\quad \left. \left. \times \left[\frac{\sqrt{A_t}}{\sqrt{1 + A_t}} \frac{\sqrt{1 + (H/H_a)} - 1}{1 - A_t/(1 + A_t)\sqrt{1 + (H/H_a)}} \right] \right\} \right].
\end{aligned} \tag{A2}
$$

Here $A_t = H_a G r_t^2$, $H'_a = H_a - H$ and $\rho_t = \rho_0 (1 - H/H_a)^{5/2}$. Note that the argument of the inverse hyperbolic tangent function may become imaginary. Then, one can use the relationship $\mathrm{artanh}(\mathrm{i}x) = \mathrm{i}\arctan(x)$. If the absolute value of the argument becomes larger than one, the inverse hyperbolic tangent function must be replaced by the inverse hyperbolic cotangent function.

References

Anthes, R. A. 1982. Tropical cyclones. their evolution, structure and effects. *Amr. Meteorol. Soc. Meteorol. Monogr.* **19**(41), 208 pp.

Blumen, W. 1978. Uniform potential vorticity flow: part I. Theory of wave interactions and two-dimensional turbulence. *J. Atmos. Sci.* **35**, 774–783.

Davies, H. C., Schär, C. and Wernli, H. 1991. The palette of fronts and cyclones within a baroclinic wave development. *J. Atmos. Sci.* **48**, 1666–1689.

Drazin, P. G. 1970. Non-linear baroclinic instability of a continuous zonal flow. *Q. J. R. Meteorol. Soc.* **96**, 667–676.

Eady, E. T. 1949. Long waves and cyclone waves. *Tellus* **1**, 33–52.

Eliassen, A. 1951. Slow thermally or frictionally controlled meridional circulation in a circular vortex. *Astrophysica Norvegica* **5**, 19–60.

Eliassen, A. and Kleinschmidt, E. 1957. Dynamic meteorology. In *Handbuch der Physik: Geophysik II*, Vol. 48, Springer-Verlag, Berlin, 1–154.

Emanuel, K. A. 1986. An air–sea interaction theory for tropical cyclones. Part I: steady-state maintenance. *J. Atmos. Sci.* **43**, 585–604.

Emanuel, K. A. 1987. An air–sea interaction model of intraseasonal oscillations in the tropics. *J. Atmos. Sci.* **44**, 2324–2340.

Emanuel, K. A. 1989. The finite-amplitude nature of tropical cyclogenesis. *J. Atmos. Sci.* **46**, 3431–3456.

Emanuel, K. A. 1995. The behavior of a simple hurricane model using a convective scheme based on subcloud-layer entropy equilibrium. *J. Atmos. Sci.* **52**, 3960–3968.

Emanuel, K. A. 1997. Some aspects of hurricane inner-core dynamics and energetics. *J. Atmos. Sci.* **54**, 1014–1026.

Ertel, H. 1942. Ein neuer hydrodynamischer Wirbelsatz. *Met. Z.* **59**, 277–281.

Hack, J. J. and Schubert, W. H. 1986. Non-linear response of atmospheric vortices to heating by organized cumulus convection. *J. Atmos. Sci.* **43**, 1559–1573.

Held, I. M., Pierrehumbert, R. T., Garner, S. T. and Swanson, K. L. 1995. Surface quasi-geostrophic dynamics. *J. Fluid Mech.* **282**, 1–20.

Hoskins, B. J. 1976. Baroclinic waves and frontogenesis. Part I: introduction and Eady waves. *Q. J. R. Meteorol. Soc.* **102**, 103–122.

Hoskins, B. J. and Bretherton, F. P. 1972. Atmospheric frontogenesis models: mathematical formulation and solution. *J. Atmos. Sci.* **29**, 11–37.

Hoskins, B. J. and West, N. V. 1979. Baroclinic waves and frontogenesis. Part II: uniform potential vorticity jet flows—cold and warm fronts. *J. Atmos. Sci.* **36**, 1663–1680.

Hoskins, B. J., McIntyre, M. E. and Robertson, A. W. 1985. On the use and significance of isentropic potential vorticity maps. *Q. J. R. Meteorol. Soc.* **111**, 877–946.

Kleinschmidt, E. 1951. Grundlagen einer Theorie der tropischen Zyklonen. *Arch. Meteor. Geophys. Bioklimatol. Ser. A* **4**, 53–72.

Nakamura, N. and Held, I. M. 1989. Non-linear equilibration of two-dimensional Eady waves. *J. Atmos. Sci.* **46**, 3055–3064.

Schubert, W. H. 2004. Generalization of Ertel's potential vorticity to a moist atmosphere. *Met. Z.*, to appear.

Schubert, W. H. and Alworth, B. T. 1987. Evolution of potential vorticity in tropical cyclones *Q. J. R. Meteorol. Soc.* **113**, 147–162.

Schubert, W. H. and Hack, J. J. 1983. Transformed Eliassen balanced vortex model. *J. Atmos. Sci.* **40**, 1571–1583.

Shutts, G. J. 1981. Hurricane structure and the zero potential vorticity approximation. *Mon. Wea. Rev.* **109**, 324–329.

Thorpe, A. J. 1985. Diagnosis of balanced vortex structure using potential vorticity. *J. Atmos. Sci.* **42**, 397–406.

Willoughby, H. E., Jin, H. L., Lord, S. J. and Piotrowicz, J. M. 1984. Hurricane structure and evolution as simulated by an axisymmetric nonhydrostatic numerical model. *J. Atmos. Sci.* **41**, 1169–1186.